Published in final edited form as:
ACS Chem Biol. 2013 September 20; 8(9): 2063–2071. doi:10.1021/cb400258d.

Avidity Modulation of Folate-Targeted Multivalent Dendrimers for Evaluating Biophysical Models of Cancer Targeting Nanoparticles

Justin E. Silpe[1,2], **Madhuresh Sumit**[1,3], **Thommey P. Thomas**[1,4], **Baohua Huang**[1,4], **Alina Kotlyar**[1,4], **Mallory A. van Dongen**[1,5], **Mark M. Banaszak Holl**[1,2,3,5,*], **Bradford G. Orr**[1,6,*], and **Seok Ki Choi**[1,4,*]

[1]Michigan Nanotechnology Institute for Medicine and Biological Sciences, University of Michigan, Ann Arbor, MI 48109, USA

[2]Macromolecular Science and Engineering, University of Michigan, Ann Arbor, MI 48109, USA

[3]Program in Biomedical Sciences, University of Michigan, Ann Arbor, MI 48109, USA

[4]Department of Internal Medicine, University of Michigan, Ann Arbor, MI 48109, USA

[5]Department of Chemistry, University of Michigan, Ann Arbor, MI 48109, USA

[6]Department of Physics, University of Michigan, Ann Arbor, MI 48109, USA

Abstract

We investigated two types of generation 5 polyamidoamine (PAMAM) dendrimers, each conjugated stochastically with a mean number of five or ten methotrexate (MTX) ligands per dendrimer (G5-MTX_5, G5-MTX_{10}), for their binding to surface-immobilized folate binding protein (FBP) as a function of receptor density. The binding study was performed under flow by surface plasmon resonance spectroscopy. Two multivalent models were examined to simulate binding of the dendrimer to the receptor surface, showing that at relatively high receptor density, both dendrimer conjugates exhibit high avidity. However, upon reducing the receptor density by a factor of three and thirteen relative to the high density level, the avidity of the lower-valent G5-MTX_5 decreases by up to several orders of magnitude (K_D = nM to μM), whereas the avidity of G5-MTX_{10} remains largely unaffected regardless of the density variation. Notably, on the 13-fold reduced FBP surface, G5-MTX_5 displays binding kinetics similar to that of monovalent methotrexate, which is patently different from the still tight binding of the higher-valent G5-MTX_{10}. Thus, the binding analysis demonstrates that avidity displayed by multivalent MTX conjugates varies in response to the receptor density, and it can be modulated for achieving tighter, more specific binding to the higher receptor density by modulation of ligand valency. We believe this study provides experimental evidence supportive of the mechanistic hypothesis of multivalent NP uptake to a cancer cell over a healthy cell where the diseased cell expresses the folate receptor at higher density.

Keywords

Folate Receptor; Methotrexate; Targeted Delivery; Multivalency; Receptor Density; Surface Plasmon Resonance Spectroscopy

*To whom correspondence should be addressed, Phone: (734) 763-2283; mbanasza@umich.edu. Phone: (734) 936-3609; orr@umich.edu. Phone: (734) 615-0618; skchoi@umich.edu.

Supporting Information Available: This material is available free of charge via the Internet at http://pubs.acs.org.

Cellular uptake of multivalent nanomaterial in drug delivery[1–4] depends on strong nanomaterial-surface adhesion over a period sufficient to achieve endocytosis under laminar and disturbed shear flows[5] through vascular endothelium. The central hypothesis of this strategy is that the nanomaterial will adhere more tightly and selectively via multivalent receptor-ligand interactions to a targeted cell surface with a higher receptor density (Figure 1). Although a large body of related studies suggests such a critical role played by the multivalent mechanism,[6–10] biophysical models that relate cell specificity of nanomaterial adhesion and surface receptor density remain poorly defined for tumor-associated receptors. In this article, we analyze binding avidity and kinetic models for the nanomaterial adsorption to a folate receptor surface by using multivalent dendrimer nanoparticles (NPs), and provide evidence supportive of the current hypothesis central to cancer cell-targeted drug delivery.

Nanomaterial applications for cancer-targeted delivery of therapeutic molecules and imaging agents have been explored by aiming a diverse array of tumor biomarkers found on the cell surface that include folic acid receptor (FAR),[11, 12] riboflavin receptor,[13, 14] $\alpha_v\beta_3$ integrin,[15–17] prostate-specific membrane antigen,[18] and epidermal growth factor receptor.[4, 19] Of those receptors, FAR has been studied most extensively for targeted delivery,[2, 20] in part due to facile access to its high affinity ligand, folic acid (FA, Figure 2) (K_D = 0.4 nM),[21] and to its well-established ability to undergo receptor-mediated endocytosis with bound FA-conjugated nanomaterials.[2] In addition, with wider implications from cancers to inflammatory diseases, FAR remains an important route for targeted delivery of diverse cytotoxic agents, which display otherwise low therapeutic indices.[11, 20]

We have been interested in examining the hypotheses of such cell-targeted multivalent strategies for developing anticancer nanotherapeutics.[22, 23] In our earlier reports, we investigated the strategy for FAR targeting by methotrexate (MTX, Figure 2) in lieu of folic acid.[22, 23] MTX belongs to the class of antifolate molecules, each having dual activities.[21, 24–26] First, it has cytotoxicity due to its ability to inhibit several metabolic enzymes localized in cytosol, primarily, dihydrofolate reductase (DHFR; K_i = 1.2 nM).[26] Second, it has a high structural homology to FA, which confers the molecular capability to bind FAR, though at a substantially lowered affinity (K_D = ~20–100 nM).[21, 24, 25] Thus, MTX serves as a small molecule ligand for FAR targeting. Despite its lower affinity as a targeting ligand for the nanomaterial delivery, we showed that its suboptimal affinity could be enhanced by several orders of magnitude for tight adsorption to a surface of high receptor density (diseased cell) via a multivalent mechanism (Figure 1b).[22, 23] In addition, its lower affinity may help reduce the level of undesired monovalent adsorption to cell surfaces of low receptor density (Figure 1a) as predicted by a theoretical analysis that multivalent cooperativity can be kinetically limited if the binding of an individual receptor-ligand pair is too tight.[27] Therefore it is possible that the targeting specificity for a particular cell type can be enhanced by making the affinity of each individual receptor-ligand pair weaker.[27–29]

In the present study, we investigate the hypothesis that cancer cell-targeted selectivity is primarily attributable to higher receptor density on the cancer cell surface.[27–29] The hypothetical notion that receptor density plays an essential role in modulating multivalent avidity has been validated in numerous biological systems that include cell adhesion,[9, 10] cell signal transduction,[7, 30] carbohydrate-lectin interaction,[8, 31–34] antibiotic-cell wall recognition,[35–37] and phage display.[38, 39] However, this mechanistic basis remains a subject of significant interest in targeted drug delivery.[6, 7, 9, 22] Certain theoretical studies propose models for specific adsorption of multivalent targeted NPs to the cancer cell that expresses specific target receptors in higher density.[27–29] These theoretical analyses predict that cell targeting specificity is primarily determined by binding avidity of a NP which increases in a

non-linear, exponential manner in response to a linear increase in the number of participating receptor-ligand pairs.

Despite the importance of such theoretical models, the claim to a single, unifying theory is largely unmet by the paucity of experimental methods capable of controlling receptor density on the cell surface and of studying the fast kinetics of multivalent binding in cell based assays. Here, we employed a model surface for the FAR-expressing cell at various receptor densities and studied binding kinetics of MTX-conjugated multivalent dendrimer NPs to the model surfaces by surface plasmon resonance (SPR) spectroscopy. This study aims to determine experimentally how the receptor density influences multivalent binding avidity, and ligand valency relates to surface specificity. It provides clear experimental evidence that receptor density plays a key role in modulation of NP avidity.

RESULTS AND DISCUSSION

Time dependence of dendrimer binding to cell surface receptors

In our earlier study,[23] we investigated the FAR-specific binding/uptake of G5-MTX_{10} in FAR-expressing cells by using a fluorescently labeled G5-$5T_3$-MTX_{10} (Figure 2). This MTX-conjugated dendrimer is selectively bound to and taken up into FAR-positive KB cancer cells but not by FAR-negative B16-F10 cells. Such cell binding occurs by a FAR-specific mechanism such that it is competitively blocked by co-incubating with free folic acid.[23] However our earlier cell study lacks information on time dependent conjugate uptake by cancer cells since it was performed under a prolonged incubation condition taking up to three days. In the present study, we further extended such cell-based binding experiments under shorter incubation periods to evaluate whether this modified condition can be used to generate data for determining cellular binding kinetics of MTX-conjugated multivalent dendrimers. With the same G5-$5T_3$-MTX_{10}, we measured its cellular uptake in FAR-overexpressing KB cells by two standard methods, flow cytometry and confocal microscopy. First, the flow cytometric results (Figure 3a) confirm the dose- and time-dependence of conjugate binding to KB cells. Second, confocal microscopic images (Figure 3b) provide qualitative evidence for the cellular internalization of the G5-$5T_3$-MTX_{10} (red fluorescence) that occurs as a function of incubation time. However, results obtained by both flow cytometry and confocal microscopy provide only poor time resolution and low detection sensitivity that make these assays unsuitable for quantitative analysis of cellular binding kinetics.

SPR spectroscopy

SPR spectroscopy enables the study of fast biomolecular events to elucidate kinetic constants from such interactions as the binding of a free-flowing conjugate, subject to shear flow, with a targeted cell immobilized on a neighboring surface. A model surface for the mammalian cell that expresses folate receptors was prepared for surface plasmon resonance experiments by immobilization of soluble folate binding protein (FBP, bovine) on the surface of a CM5 sensor chip. The protein immobilization was carried out by an EDC-based amide coupling method as described elsewhere,[6] and three FBP-presenting chips were prepared by varying the protein density at 14.7, 4.8, or 1.1 FBP ng/mm^2 (Supplementary Figure S2a; 1000 RU (response unit) = 1 ng protein/mm^2). These FBP densities are equivalent to the number densities of ~3×10^{11}, 1×10^{11}, 2×10^{10} FBP molecules per mm^2, respectively, which vary over a 13-fold range. This magnitude of variation in protein density is comparable to the overexpression ratio of folate receptors implicated in certain cancers such as ovarian and endometrial cancers in which the receptor density is 10- to 20-fold higher in the malignant cells than normal epithelial cells in the same tissue.[40, 41] In addition, the high end of the FBP density on a current sensor chip closely approaches the surface

density of folate receptors expressed on several malignant cell lines.[41] According to a radioligand (^{3}H-labeled FA) binding assay, approximately ≥20 pmol folate receptors are detected on average per 10^6 cells,[41] a surface density which is translated to ~10^{10}–10^{11} receptor molecules per mm^2 (≈ 0.1–1 receptor molecule per 10 nm^2) when calculated on an assumption that a malignant cell has a radius (r) of 5–10 μm and its accessible surface area is $2\pi r^2$.[40, 41] Thus, the range of FBP densities provided by those three sensor chips appears to address the variation in surface density of folate receptors between normal cells and malignant cells.[41]

Each sensor chip was first assessed for its binding specificity by injecting FA and MTX ligands (Supplementary Figure S2b,c). Based on a 1:1 binding mode (monovalent) for free FA or MTX, analysis by a Langmuir model[6] was applied to each sensorgram, and kinetic parameters for the receptor-ligand interaction (on rate = k_{on}, off rate = k_{off}) were extracted by global curve fittings according to BIAevaluation software (version 3). Equilibrium dissociation constants ($K_D = k_{off}/k_{on}$) for FA and MTX were determined on average for three FBP densities, confirming that MTX binds to bovine FBP with a lower affinity (K_D = 4×10^{-5} M) than FA ($K_D = 2 \times 10^{-6}$ M in this study; $K_D = 5\ (\pm 3) \times 10^{-6}$ M (lit.)[6]) primarily as a result of its greater off rate.

Binding of G5-MTX$_n$ to high receptor density

SPR binding studies were performed for G5-MTX$_n$ (n = 5, 10), each at three different receptor densities (Figure 4, Supplementary Figure S3, S4). First, each MTX conjugate binds to the FBP surface at (sub)micromolar concentrations as low as 0.1 μM, at which a monovalent ligand, FA or MTX, shows no detectable response. Second, each conjugate has a specific binding activity (Supplementary Figure S3). It shows a high level of adsorption to the FBP surface (flow cell 1), with no specific binding to the reference surface (flow cell 2) other than a slight positive bulk effect. In contrast, G5-MTX$_0$—the parent cyclooctyne-conjugated dendrimer not clicked with MTX—failed to show any meaningful level of adsorption to the otherwise identical sensor chip (Figure 4C). Third, the adsorption level of dendrimer conjugates, when injected at an identical concentration, is correlated with their MTX valency (n) in a manner that greater adsorption occurs at higher multivalency (ΔRU (n = 10) > ΔRU (n = 5)). The result is qualitatively indicative of tighter binding by G5-MTX$_{10}$ than G5-MTX$_5$ to the high FBP surface.

Each sensorgram acquired by each MTX conjugate (Figure 4) shows binding kinetics characterized by markedly slow dissociation (desorption) relative to the rapid dissociation displayed by either free FA or MTX (Supplementary Figure S2). In our earlier study, we also observed similar, slow dissociation profiles from G5-FA$_n$ ($n \geq 3$), a folate-presenting multivalent PAMAM dendrimer.[6] Such slow dissociation is commonly responsible for tight binding (low K_D), as associated in numerous other multivalent systems.[35–37] In addition, each conjugates' dissociation appears to occur in more than one phase, initially at a rapid off-rate (= Δ(ΔRU) ÷ Δt), and subsequently at a slower off-rate. This dissociation feature is illustrated by time-dependent fractional desorption (= RU_D/RU_A), which is defined as the mass of the dendrimer desorbed (RU_D) relative to the total mass of the dendrimer adsorbed (RU_A). For example, G5-MTX$_{10}$ showed approximately 25% fractional desorption per initial 25s in a dissociation phase and followed by only an additional 8% of fractional desorption per following 25–50s while the dissociation appears to be still incomplete (collectively ~50%) at the end of data collection time (300s).

Effect of receptor density

In order to determine how receptor density influences multivalent interaction with G5-MTX$_n$ under a flow condition, we continued SPR studies using two other sensor chips, each

immobilized with a different level of FBP. Each of these chips presents FBP on the surface in ~3- or 13-fold lower density, respectively, than the high density chip. Dose-dependent binding sensorgrams were acquired for each chip (Supplementary Figure S4), and selected sensorgrams illustrate the effect of receptor density on the dendrimer interaction (Figure 4). With injection concentration being constant, each conjugate is substantially different in both adsorption level (RU_A) and kinetic binding features, in particular, in the dissociation phase. Values of RU_A for G5-MTX_{10} decrease in response to the FBP density in a manner linearly proportional to the ratio between the receptor densities ($[FBP]_{high}/[FBP]_{low} \approx 10$; $([FBP]_{high}/[FBP]_{intermediate} \approx 2$). However, the values of fractional desorption by this conjugate remain almost unchanged regardless of the variation in receptor density (Figure 5). The latter observation suggests that G5-MTX_{10} binds to the surface in lower receptor density as tightly as to the higher density surface, while its absolute mass of adsorption (RU_A) is smaller in the lower density, possibly, because of lower number of surface receptor molecules available for interaction.

The other conjugate, G5-MTX_5, showed a similar trend in values of adsorption (RU_A) that vary in response with respect to receptor density. However, in contrast to G5-MTX_{10}, the fractional desorption displayed by this lower-valency conjugate is largely determined by the receptor density. It suggests that G5-MTX_5, bound to the surface of lower receptor density, dissociates faster than when it was bound to the higher density surface. As an illustration, G5-MTX_5 showed approximately 90% of fractional desorption per initial 150s in the dissociation phase, which is greater than ~65% and ~45% of fractional desorption, each observed in the intermediate and high density surface, respectively (Figure 5). Thus, the decrease in receptor density reduces not only the mass of dendrimer particles adsorbed to the surface but the overall strength of dendrimer-surface interaction. We believe this is qualitatively supportive of the mechanism in cell-targeted delivery by which certain multivalent nanoparticles adhere more tightly, and therefore, more selectively, to the cell surface with higher receptor density.

Two proposed models for surface adsorption of stochastic dendrimers

Qualitative analysis of SPR results points to FBP density as a primary parameter that promotes adsorption of the multivalent MTX conjugate. In an effort to quantitatively analyze this observation, we developed two potential models for interpreting the binding kinetics of stochastic dendrimer species to a FBP model using the number of free FBP sites as a dynamic variable.

Surface conversion model

This kinetic model is based on a series of reversible binding events that occur in a sequence on the surface. As an illustration, an MTX-conjugated dendrimer G5-MTX_n comes down under flow and adheres to the FBP surface, forming a monovalent species A as a result of making a single receptor-ligand interaction with a certain rate constant (k_{a1}; Figure 6). Once adsorbed, species A can then desorb to an unbound state (k_{d1}) or convert to a multivalent-bound state, forming species B (k_{a2}). In this model, if the dendrimer has too few MTX ligands, or if the density of receptors on the surface is too low, then it may not be possible for all species A to convert to species B. In this continuum model, we assume that there is no direct desorption of B to a free state (k_{d3}) without following the microscopic reverse pathway to A.

In order to fit this model, we introduced a set of coupled differential equations that describe the evolution of the number of free receptor sites, and derived the rate of change of the mass of species A, and B (for details, see the Materials and Methods section). The fitting was performed by numerical integration of the model (Supplementary Figure S5 and S6), and

the best fits allowed us to extract two pairs of rate constants involved in this binding model (Table 1). These kinetic parameters suggest a number of physical implications important for understanding the dendrimer-surface interaction. First, in the analysis of on–rates as illustrated by G5-MTX_{10}, the solution–to–surface association constant (k_{a1}) of the dendrimer particle is much greater than the subsequent association constant on the surface (k_{a2}) at each receptor density. Second, in the analysis of off-rates, the surface–to–solution dissociation constants of species A (k_{d1}) are ~30- to 80-fold greater than the dissociation constants of species B (k_{d2}) per receptor density.

For an equilibrium analysis of G5-MTX_{10}, each pair of opposite rate constants was used to calculate an equilibrium dissociation constant ($K_{D1,\ monovalent} = k_{d1}/k_{a1}$) for one subpopulation of the bound conjugate (species A), and also a multivalent dissociation constant ($K_{D,\ multivalent} = K_{D1} \times K_{D2}$) for the other subpopulation (species B). Of those two subpopulations, the multivalent species B constitutes a major fraction of the total conjugate bound in each FBP surface, and binds tightly with the (sub)nanomolar $K_{D,\ multivalent}$ value. In contrast, the monovalent species A, that constitutes a minor fraction, binds weakly at the micromolar range of K_{D1} values. The variation in receptor density had only a minimal effect on the binding kinetics of G5-MTX_{10}, suggesting that the valency ($n = 10$) of MTX ligands presented on the dendrimer surface provides a ligand density which is sufficiently high to counterbalance the effect caused by the decrease in receptor density.

The same analysis was performed for the binding of G5-MTX_5 to various FBP densities. G5-MTX_5 showed slightly similar trends compared to those observed with G5-MTX_{10} above, but its kinetic features were entirely distinct at the low FBP density. The species B, determined from the adsorption of G5-MTX_5 to a high or intermediate FBP surface, bound as tightly as the species B from G5-MTX_{10}. However, its fractions were generally lower and decreased in response to the decrease in FBP density. In addition, species A played a more significant role in G5-MTX_5, and it became a major population in adsorption to the FBP surface even in the intermediate density. Compared to G5-MTX_{10}, the total mass of adsorption, which is expressed as the sum of fractions A and B, is lowered with G5-MTX_5. All of these results suggest that the lower-valent conjugate binds less tightly than the higher-valent conjugate when tested in an otherwise identical condition. It is highly remarkable to see that species A is almost an exclusive species from G5-MTX_5 in a low FBP surface. This analysis suggests that G5-MTX_5 adsorbs to the low FBP surface in a monovalent manner with a K_D value of 9 μM. Thus variation in receptor density made a more significant effect for G5-MTX_5, in particular, on a low receptor surface. It is clear that even 2-fold decrease in ligand valency (G5-MTX_5 vs G5-MTX_{10}) may be sufficient to cause different responses to variation in receptor density.

Dual Langmuir model

In the earlier model based on surface conversion, we analyzed dendrimer adhesion under a condition where there is no direct desorption of a multivalent B species to a free dendrimer. In this model (Figure 6), we try to address the heterogeneity and physical barriers present on the FBP surface that prevents conversion between species B and species A. Thus, we hypothesize that each species A or B—bound either weakly or tightly respectively—adsorbs independently, and can desorb to a free state without need for direct conversion from species A to species B or the reverse. The solution for this dual dissociation model is just the sum of two independent exponential decay functions for species A and B and was obtained according to the Langmuir isotherm (see details in the Materials and Methods section).

In the analysis of the association phase, this model faces a limitation due to lack of experimental data and/or a mathematical method that allows the determination of two on-rate constants, independently, for species A and B. However, since the on-rate for dendrimer

adsorption is largely governed by the first association event, the solution–to–surface association (k_{a1}), which is much faster than those subsequent steps occurring on the surface (Table 1), we assumed that on-rate constants for the formation of two independent species A and B would be almost identical ($k_{a1} \approx k_{a2}$). Accordingly, kinetic rate constants, and equilibrium dissociation constants were extracted for each bound species A and B (Supplementary Table S1).

Binding features derived from this dual Langmuir model are highly consistent with those associated with the surface conversion model. First, adsorption of G5-MTX_{10} generates species B as a major fraction (~70%) in each of the FBP surfaces. The species B binds two orders of magnitude more tightly ($K_{D,2} \approx 10^{-8}$) than the other species A. Such tighter binding is observed consistently and little affected by variation in receptor density. In contrast, adsorption of G5-MTX_5 showed different trends in response to variation in FBP density. In this lower-valent conjugate, species B constitutes slightly a major fraction (~60%) only in one surface (high FBP density), and binds one order of magnitude more tightly ($K_{D,2} \approx 10^{-7}$) than the other species A. However, species A constitutes a major subpopulation in the intermediate as well as low FBP surface. Thus, this model is generally consistent with the conversion model, and supportive of a trend that the lower-valent conjugate binds less tightly than the higher-valent conjugate, and its surface adsorption decreases significantly in response to decrease in receptor density.

Implications for cell targeting

Our SPR binding results combined with kinetic analysis performed with two biophysical adsorption models provide unique insights that are strongly supportive of a multivalent strategy for cancer cell targeting. First, we correlate the total mass of dendrimer adsorbed to the surface with the density of FBP immobilized on the sensor chip surface (Figure 7). The receptor density constitutes one of the critical biological indicators that distinguish between a normal cell and a malignant cell. In this study, the receptor density varies approximately 13-fold from ~2.3×10^{10} (relatively low density) to 1.0×10^{11} (intermediate) to 3.1×10^{11} (high), each expressed as number of FBP molecules per mm^2. G5-MTX_5 clearly shows a positive correlation where its ΔRU value (normalized) increases from 3 (low density; density ratio = 1) to 19 (intermediate; density ratio = 4.4) to 51 (high; density ratio = 13.4) in response to receptor density (Figure 7). G5-MTX_{10} shows a lower adsorption at the low density (ΔRU = 16), and reaches a saturation level at the intermediate and high density. We believe that these differences in the saturation level are determined by fractions of both species A and species B as well as by the affinity of species A (Table 1). For example, the combined fraction is greater for G5-MTX_{10} (74%) than G5-MTX_5 (22%) at the intermediate receptor density. In addition, the affinity of species A is greater for G5-MTX_{10} (K_{D1} = 2–8 μM) than G5-MTX5 (K_{D1} = 7–17 μM), contributing to faster saturation by G5-MTX_{10}. Despite such differences observed between G5-MTX_5 and G5-MTX_{10}, it is clear that the surface that presents FBP in higher density allows for a greater level of dendrimer adsorption. This could serve an important piece of evidence which points to a cancer cell-directed selective adsorption by folate-targeted dendrimer nanoparticles.

Second, we performed fractional analysis for species B relative to a total mass of dendrimer species adsorbed (A and B) at the end of each association phase as illustrated in a surface conversion model (Figure 7), and in a dual Langmuir model (Supplementary Figure S7). In each of the binding models, species B represents a group of those dendrimer nanoparticles that bind more tightly than the nanoparticles of species A. The particles of species B are characterized to be able to provide a longer duration of surface attachment due to their slower desorption rates, and therefore might afford a greater probability of being taken up by the cell via the FAR-mediated endocytosis.[2] We observed a remarkable distinction between G5-MTX_{10} and G5-MTX_5 such that the former dendrimer binds to the FBP surface by

forming mostly species B (58–72%) with little variation by the receptor density. However the latter dendrimer adsorbs to the surface via species B (5–57%) formed in a manner dependent on the receptor density. In addition, the mechanism of adsorption by G5-MTX_5 to the low density surface occurs almost exclusively via formation of species A which dissociate relatively fast.

This fractional analysis suggests that cancer cell targeting by a multivalent dendrimer might be also accounted for by tighter adsorption that occurs at the surface at a higher receptor density. G5-MTX_{10} appears to be less desirable than G5-MTX_5 for cancer cell targeting due to its still high fraction of species B to the low density surface (a model for a normal cell). However, it should be noted that the normalized mass of G5-MTX_{10} adsorbed to the low density (ΔRU = 16%; fraction of species B = 0.58) is still ~6-fold lower than the adsorption to the high density surface (ΔRU = 100%; fraction of species B = 0.63; Figure 7). G5-MTX_5 appears to provide a greater selectivity in cell targeting by showing both stronger adsorption to the high density surface (ΔRU = 51%; fraction of species B = 0.51) and a weaker adsorption to the low density chip (ΔRU = 3%; fraction of species A ≥0.95). However, G5-MTX5 adsorbs less in mass to the higher density surface ~2–fold (high density) or ~6-fold (intermediate density) than G5-MTX_{10}. Clearly this is a disadvantage with respect to the total amount of dendrimer nanoparticles that can be delivered to a broad range of cancer cells, each presenting FAR in a variable density.

CONCLUSION

In summary, we studied SPR binding kinetics of two multivalent dendrimer NPs G5-$(MTX)_n$ (n = 5, 10) to the model surface of three receptor densities based on a FAR-expressing cell. We considered two complimentary kinetic models to analyze the adsorption of dendrimer NPs with the surface and extracted kinetic parameters to deduce rate constants and distributions of adsorbed NP populations. First, the surface binding was greater for the higher-valent G5-MTX_{10}, which is correlated with our earlier study[23] showing its higher uptake and cytotoxicity in FAR-positive KB cells *in vitro*. Second, variation in the receptor density substantially influences the binding avidity of dendrimer NPs as illustrated with G5-MTX_5, which shows enhancement in avidity over three orders of magnitude in response to ~13-fold variation in receptor density. Therefore, the present study provides experimental evidence supportive of the hypothetical notion that receptor overexpression on the cancer cell surface serves a key parameter in the multivalent design of nanomaterials for cancer diagnostics and drug delivery.[27–29] It also supports a mechanistic hypothesis related to the adsorption models raised in literature;[27–29] multivalent mechanisms introduce non-linear effects in the receptor density-avidity relationship that cannot be accounted for by additive effects alone. Finally, the current work shows that avidity varies as a function of both receptor density and ligand valency as demonstrated with a higher-valent G5-MTX_{10}, which constitutively exhibits nanomolar binding avidity even to the surface at the lowest receptor density. Thus cell targeting capability is modulated through specific features in the design of multivalent nanomaterials. In consideration of these observations together, the current work provides implications of significant importance to the continued development and better understanding of multivalent nanomaterials for targeting those receptor biomarkers overexpressed in cancers and other serious diseases.

METHODS

Full details for materials and methods (cell culture, flow cytometry, confocal microscopy, SPR spectroscopy) are provided in the Supporting Information (Page S2–S5) and references cited therein. Protein immobilization and data acquisition for SPR experiments (Page S3) were performed as described elsewhere.[6, 22, 37] Analysis of SPR data was performed by

fitting to two biophysical models, surface conversion and dual Langmuir, each analyzed according to those assumptions and fitting parameters described in details (Page S5).

Supplementary Material

Refer to Web version on PubMed Central for supplementary material.

Acknowledgments

This work has been supported by the National Cancer Institute, National Institutes of Health under award 1 R01 CA119409. J.S. received fellowship support from Undergraduate Research Opportunity Program at University of Michigan.

References

1. Kukowska-Latallo JF, Candido KA, Cao Z, Nigavekar SS, Majoros IJ, Thomas TP, Balogh LP, Khan MK, Baker JR Jr. Nanoparticle Targeting of Anticancer Drug Improves Therapeutic Response in Animal Model of Human Epithelial Cancer. Cancer Res. 2005; 65:5317–5324. [PubMed: 15958579]
2. Low PS, Henne WA, Doorneweerd DD. Discovery and Development of Folic-Acid-Based Receptor Targeting for Imaging and Therapy of Cancer and Inflammatory Diseases. Acc Chem Res. 2008; 41:120–129. [PubMed: 17655275]
3. Dhar S, Gu FX, Langer R, Farokhzad OC, Lippard SJ. Targeted delivery of cisplatin to prostate cancer cells by aptamer functionalized Pt(IV) prodrug-PLGA-PEG nanoparticles. Proc Natl Acad Sci U S A. 2008; 105:17356–17361. [PubMed: 18978032]
4. Bhirde AA, Patel V, Gavard J, Zhang G, Sousa AA, Masedunskas A, Leapman RD, Weigert R, Gutkind JS, Rusling JF. Targeted Killing of Cancer Cells in Vivo and in Vitro with EGF-Directed Carbon Nanotube-Based Drug Delivery. ACS Nano. 2009; 3:307–316. [PubMed: 19236065]
5. Chiu JJ, Chien S. Effects of Disturbed Flow on Vascular Endothelium: Pathophysiological Basis and Clinical Perspectives. Physiol Rev. 2011; 91:327–387. [PubMed: 21248169]
6. Hong S, Leroueil PR, Majoros IJ, Orr BG, Baker JR Jr, Banaszak Holl MM. The Binding Avidity of a Nanoparticle-Based Multivalent Targeted Drug Delivery Platform. Chem Biol (Oxford, U K). 2007; 14:107–115.
7. Kiessling LL, Gestwicki JE, Strong LE. Synthetic Multivalent Ligands in the Exploration of Cell-Surface Interactions. Curr Opin Chem Biol. 2000; 4:696–703. [PubMed: 11102876]
8. Lee YC, Lee RT. Carbohydrate-Protein Interactions: Basis of Glycobiology. Acc Chem Res. 1995; 28:321–327.
9. Mammen M, Choi SK, Whitesides GM. Polyvalent Interactions in Biological Systems: Implications for Design and Use of Multivalent Ligands and Inhibitors. Angew Chem, Int Ed Engl. 1998; 37:2754–2794.
10. Roy R. Syntheses and Some Applications of Chemically Defined Multivalent Glycoconjugates. Curr Opin Struct Biol. 1996; 6:692–702. [PubMed: 8913693]
11. Hilgenbrink AR, Low PS. Folate receptor-mediated drug targeting: From therapeutics to diagnostics. J Pharm Sci. 2005; 94:2135–2146. [PubMed: 16136558]
12. Lee RJ, Low PS. Folate-mediated tumor cell targeting of liposome-entrapped doxorubicin in vitro. Biochim Biophys Acta (BBA) - Biomembranes. 1995; 1233:134–144.
13. Thomas TP, Choi SK, Li MH, Kotlyar A, Baker JR Jr. Design of Riboflavin-Presenting PAMAM Dendrimers as a New Nanoplatform for Cancer-Targeted Delivery. Bioorg Med Chem Lett. 2010; 20:5191–5194. [PubMed: 20659800]
14. Plantinga A, Witte A, Li MH, Harmon A, Choi SK, Banaszak Holl MM, Orr BG, Baker JR Jr, Sinniah K. Bioanalytical Screening of Riboflavin Antagonists for Targeted Drug Delivery—A Thermodynamic and Kinetic Study. ACS Med Chem Lett. 2011; 2:363–367. [PubMed: 21686082]

15. Montet X, Funovics M, Montet-Abou K, Weissleder R, Josephson L. Multivalent Effects of RGD Peptides Obtained by Nanoparticle Display. J Med Chem. 2006; 49:6087–6093. [PubMed: 17004722]

16. Shukla R, Thomas TP, Peters J, Kotlyar A, Myc A, Baker JR Jr. Tumor angiogenic vasculature targeting with PAMAM dendrimer-RGD conjugates. Chem Commun (Cambridge, U K). 2005:5739–5741.

17. Temming K, Lacombe M, Schaapveld RQJ, Orfi L, Kéri G, Poelstra K, Molema G, Kok RJ. Rational Design of RGD–Albumin Conjugates for Targeted Delivery of the VEGF-R Kinase Inhibitor PTK787 to Angiogenic Endothelium. ChemMedChem. 2006; 1:1200–1203. [PubMed: 16991175]

18. Chen Y, Foss CA, Byun Y, Nimmagadda S, Pullambhatla M, Fox JJ, Castanares M, Lupold SE, Babich JW, Mease RC, Pomper MG. Radiohalogenated Prostate-Specific Membrane Antigen (PSMA)-Based Ureas as Imaging Agents for Prostate Cancer. J Med Chem. 2008; 51:7933–7943. [PubMed: 19053825]

19. Thomas TP, Shukla R, Kotlyar A, Liang B, Ye JY, Norris TB, Baker JR Jr. Dendrimer-Epidermal Growth Factor Conjugate Displays Superagonist Activity. Biomacromolecules. 2008; 9:603–609. [PubMed: 18193839]

20. Lu Y, Low PS. Folate-mediated delivery of macromolecular anticancer therapeutic agents. Adv Drug Deliv Rev. 2002; 54:675–693. [PubMed: 12204598]

21. Kamen BA, Capdevila A. Receptor-mediated folate accumulation is regulated by the cellular folate content. Proc Natl Acad Sci U S A. 1986; 83:5983–5987. [PubMed: 3461471]

22. Li MH, Choi SK, Thomas TP, Desai A, Lee KH, Kotlyar A, Banaszak Holl MM, Baker JR Jr. Dendrimer-Based Multivalent Methotrexates As Dual Acting Nanoconjugates for Cancer Cell Targeting. Eur J Med Chem. 2012; 47:560–572. [PubMed: 22142685]

23. Thomas TP, Huang B, Choi SK, Silpe JE, Kotlyar A, Desai AM, Gam J, Joice M, JRB. Polyvalent PAMAM-Methotrexate Dendrimer as a Folate Receptor-Targeted Therapeutic. Mol Pharmaceutics. 2012; 9:2669–2676.

24. Nandini-Kishore SG, Frazier WA. [^{3}H]Methotrexate as a ligand for the folate receptor of *Dictyostelium discoideum*. Proc Natl Acad Sci U S A. 1981; 78:7299–7303. [PubMed: 6278468]

25. Rijnboutt S, Jansen G, Posthuma G, Hynes JB, Schornagel JH, Strous GJ. Endocytosis of GPI-linked Membrane Folate Receptor-α. J Cell Biol. 1996; 132:35–47. [PubMed: 8567728]

26. Ercikan-Abali EA, Waltham MC, Dicker AP, Schweitzer BI, Gritsman H, Banerjee D, Bertino JR. Variants of human dihydrofolate reductase with substitutions at leucine-22: effect on catalytic and inhibitor binding properties. Mol Pharmacol. 1996; 49:430–437. [PubMed: 8643082]

27. Licata NA, Tkachenko AV. Kinetic Limitations of Cooperativity-Based Drug Delivery Systems. Phys Rev Lett. 2008; 100:158102. [PubMed: 18518156]

28. Martinez-Veracoechea FJ, Frenkel D. Designing super selectivity in multivalent nano-particle binding. Proc Natl Acad Sci USA. 2011; 108:10963–10968. [PubMed: 21690358]

29. Wang S, Dormidontova EE. Nanoparticle Design Optimization for Enhanced Targeting: Monte Carlo Simulations. Biomacromolecules. 2010; 11:1785–1795. [PubMed: 20536119]

30. Kiessling LL, Gestwicki JE, Strong LE. Synthetic Multivalent Ligands as Probes of Signal Transduction. Angew Chem Int Ed. 2006; 45:2348–2368.

31. Munoz EM, Correa J, Riguera R, Fernandez-Megia E. Real-Time Evaluation of Binding Mechanisms in Multivalent Interactions: A Surface Plasmon Resonance Kinetic Approach. J Am Chem Soc. 2013; 135:5966–5969. [PubMed: 23565759]

32. Kitov PI, Sadowska JM, Mulvey G, Armstrong GD, Ling H, Pannu NS, Read RJ, Bundle DR. Shiga-like toxins are neutralized by tailored multivalent carbohydrate ligands. Nature. 2000; 403:669–672. [PubMed: 10688205]

33. Simanek EE, McGarvey GJ, Jablonowski JA, Wong CH. Selectin-Carbohydrate Interactions: From Natural Ligands to Designed Mimics. Chem Rev (Washington, DC, U S). 1998; 98:833–862.

34. Dam TK, Brewer CF. Thermodynamic Studies of Lectin-Carbohydrate Interactions by Isothermal Titration Calorimetry. Chem Rev (Washington, DC, U S). 2002; 102:387–430.

35. Metallo SJ, Kane RS, Holmlin RE, Whitesides GM. Using Bifunctional Polymers Presenting Vancomycin and Fluorescein Groups To Direct Anti-Fluorescein Antibodies to Self-Assembled

Monolayers Presenting d-Alanine-d-Alanine Groups. J Am Chem Soc. 2003; 125:4534–4540. [PubMed: 12683824]

36. Rao J, Yan L, Xu B, Whitesides GM. Using Surface Plasmon Resonance to Study the Binding of Vancomycin and Its Dimer to Self-Assembled Monolayers Presenting d-Ala-d-Ala. J Am Chem Soc. 1999; 121:2629–2630.
37. Choi SK, Myc A, Silpe JE, Sumit M, Wong PT, McCarthy K, Desai AM, Thomas TP, Kotlyar A, Holl MMB, Orr BG, Baker JR. Dendrimer-Based Multivalent Vancomycin Nanoplatform for Targeting the Drug-Resistant Bacterial Surface. ACS Nano. 2013; 7:214–228. [PubMed: 23259666]
38. Bastings MMC, Helms BA, van Baal I, Hackeng TM, Merkx M, Meijer EW. From Phage Display to Dendrimer Display: Insights into Multivalent Binding. J Am Chem Soc. 2011; 133:6636–6641. [PubMed: 21473586]
39. Reulen SWA, Dankers PYW, Bomans PHH, Meijer EW, Merkx M. Collagen Targeting Using Protein-Functionalized Micelles: The Strength of Multiple Weak Interactions. J Am Chem Soc. 2009; 131:7304–7312. [PubMed: 19469576]
40. Parker N, Turk MJ, Westrick E, Lewis JD, Low PS, Leamon CP. Folate receptor expression in carcinomas and normal tissues determined by a quantitative radioligand binding assay. Anal Biochem. 2005; 338:284–293. [PubMed: 15745749]
41. Weitman SD, Lark RH, Coney LR, Fort DW, Frasca V, Zurawski VR, Kamen BA. Distribution of the Folate Receptor GP38 in Normal and Malignant Cell Lines and Tissues. Cancer Res. 1992; 52:3396–3401. [PubMed: 1596899]
42. Huang B, Desai A, Zong H, Tang S, Leroueil P, Baker JR Jr. Copper-free click conjugation of methotrexate to a PAMAM dendrimer platform. Tetrahedron Lett. 2011; 52:1411–1414. [PubMed: 21383864]

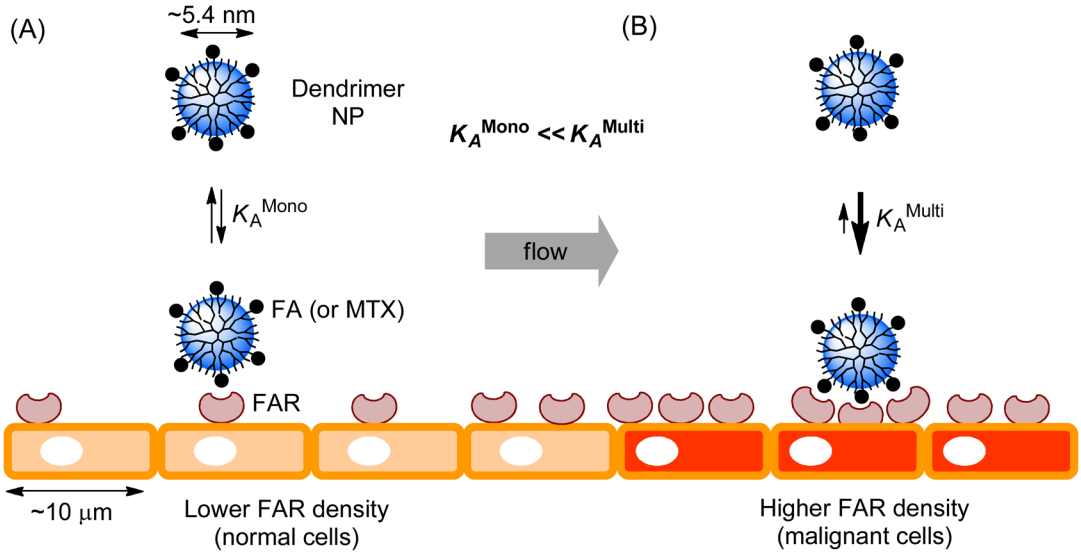

Figure 1.

Central hypothesis for folate-targeted nanoparticle (NP) delivery in cancer. It is based on a biophysical mechanism in which a folate-conjugated multivalent dendrimer NP adsorbs more strongly to the malignant cell surface expressing folate receptor (FAR) in a higher density (B) than to the normal cell (A).

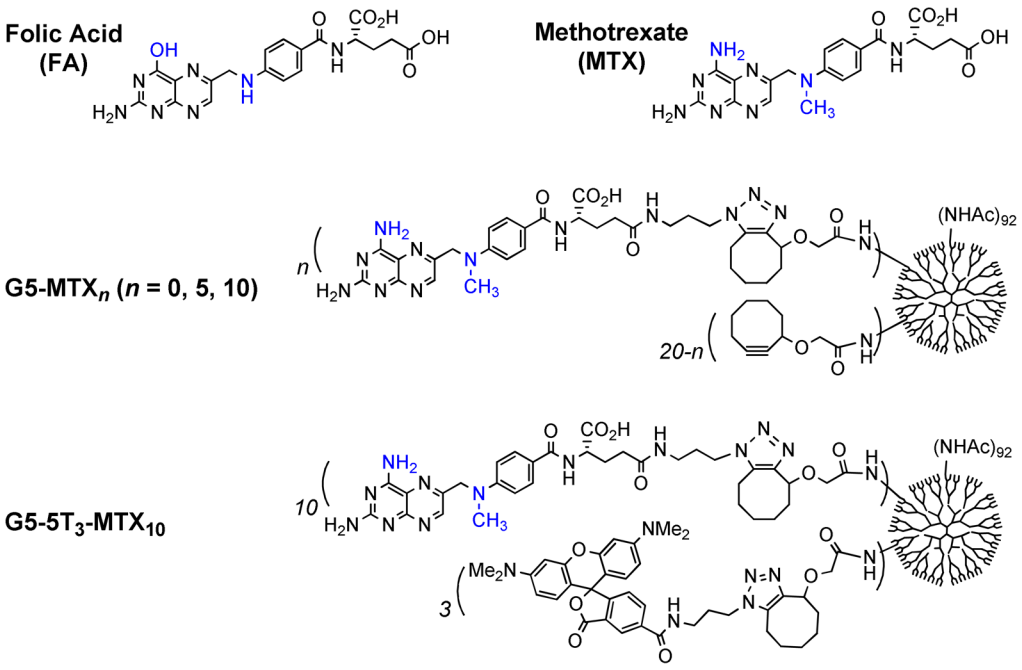

Figure 2.
Structure of folic acid, and methotrexate, and a fifth generation (G5) PAMAM dendrimer conjugates G5-MTX$_n$ and G5-5T$_3$-MTX$_{10}$.[42]

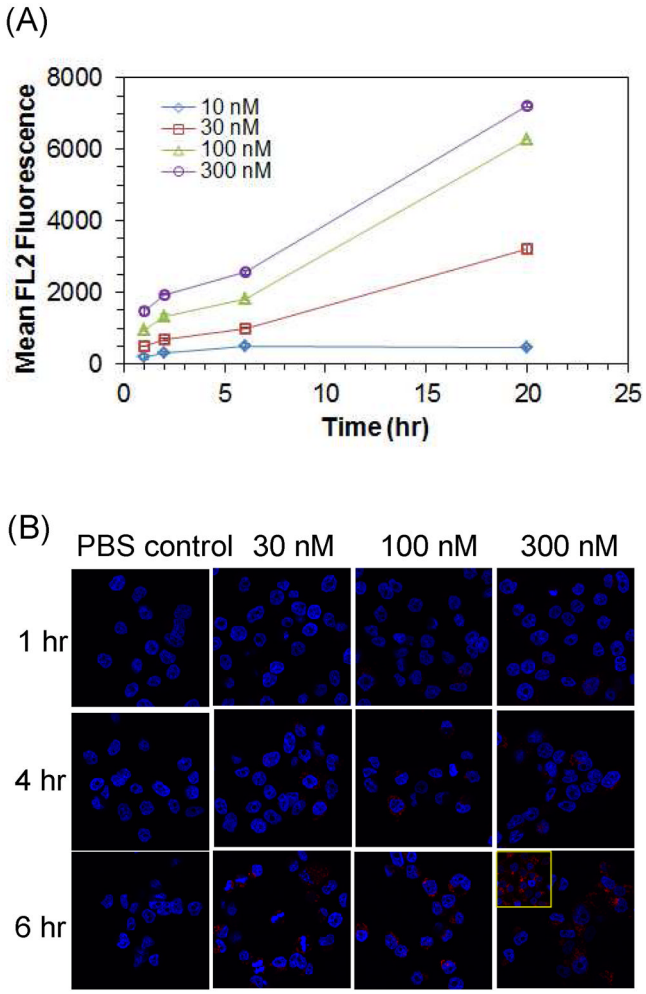

Figure 3.

Time-dependent uptake of G5-5T$_3$-MTX$_{10}$ in FAR-positive KB cancer cells measured by flow cytometry (A) and confocal fluorescence microscopy (B). The blue and the red fluorescence represent the nuclei stained with DAPI and the cytoplasm with 5TAMRA (5T) attached to dendrimer, respectively. Inset (bottom right; 20 hr)

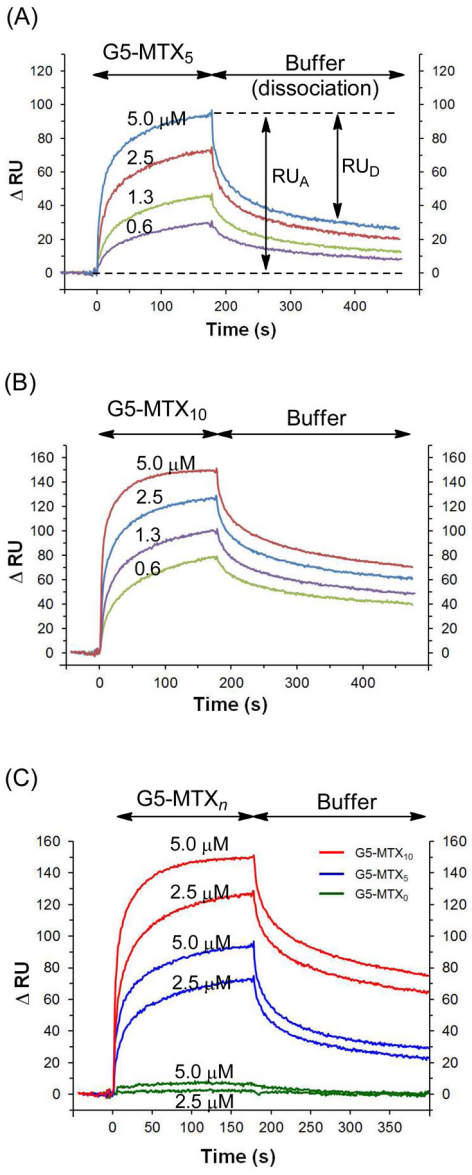

Figure 4.

Representative dose-dependent SPR sensograms of G5-MTX$_n$ (n = 0, 5, 10) in high FBP density. Each sensorgram is corrected against the reference sensorgram: $\Delta RU = RU_1$ (Fc1) − RU_2 (Fc2).

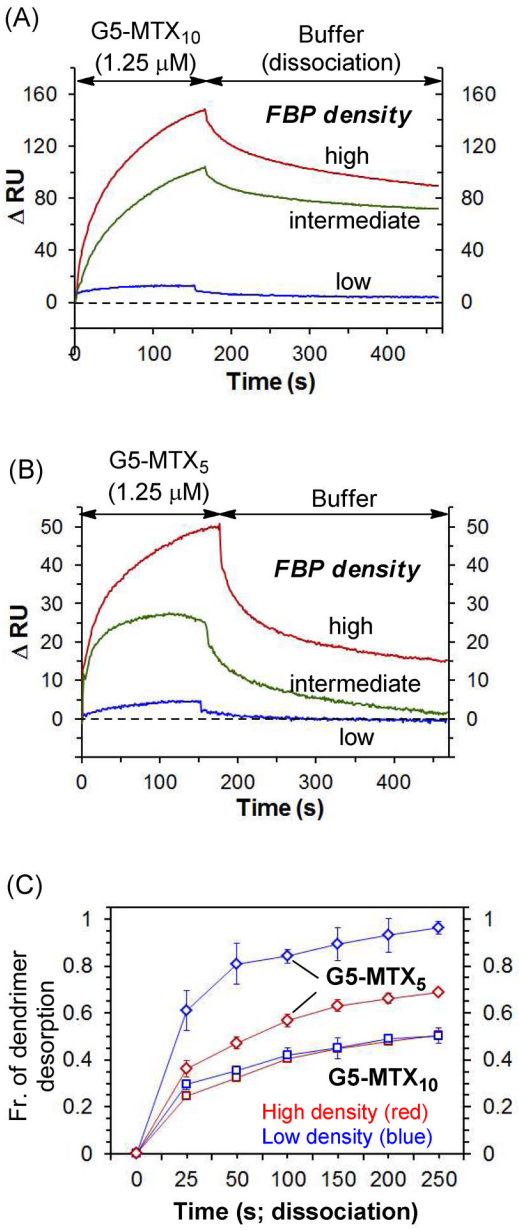

Figure 5.

Effect of receptor density on the binding kinetics of G5-MTX$_n$ (n = 5, 10). (A, B) Each plot shows average traces of sensorgrams (n = 3) obtained from the dendrimer injection at the variable level of FBP density. (C) A plot of fractional desorption of G5-MTX$_n$ in response to variation in FBP density (n = 3; mean ± SD).

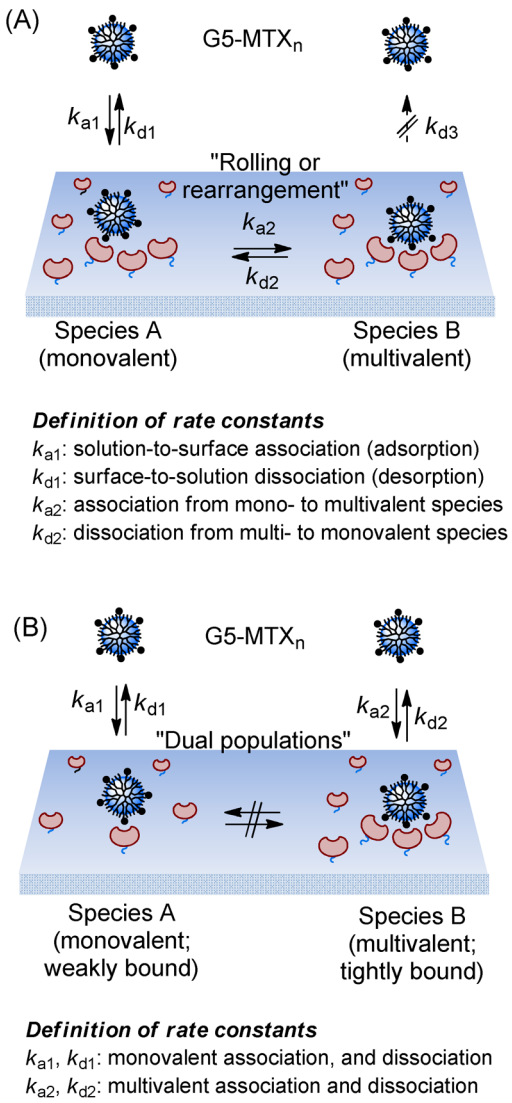

Figure 6.

Models for adsorption of G5-MTX$_n$ to surface immobilized folate binding protein (FBP) in a flow cell: surface conversion (A), dual Langmuir (B).

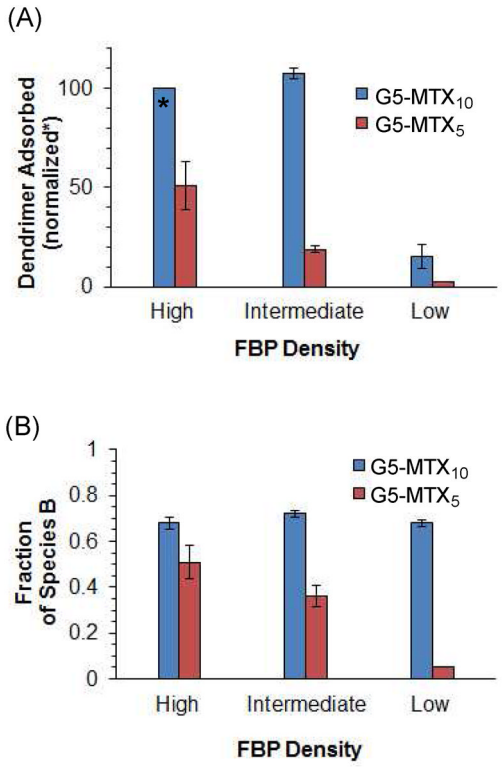

Figure 7.

Normalized mass of G5-MTX$_n$ adsorbed to the folate binding protein (FBP) surface and fraction of species B as a function of receptor density(A) Each ΔRU value (t = 175 s) was normalized relative to the value of G5-MTX$_{10}$ at the high FBP surface per identical concentration, which is arbitrarily taken as 100% (n = 3; mean ± SD). (B) Fraction of species B at the end of an association phase refers to the value extracted by the simulation in a surface conversion model (Table 1): Fraction B = Mass B ÷ (Mass A + Mass B).

Table 1

Kinetic parameters of G5-MTX$_n$ (n = 5, 10) binding to the FBP surface in a surface conversion model. Each value corresponds to the mean value calculated from three different concentrations of dendrimer injection per sensor chip ([G5-MTX$_n$] = 1.3, 2.5, 5.0 μM).

G5-MTX$_{10}$	**High density**	**Intermediate density**	**Low density**
k_{a1}	2.4(± 0.55) × 10^4	1.0(± 0.44) × 10^4	2.5(± 0.86) × 10^4
k_{d1}	5.2(± 0.9) × 10^{-2}	2.9 × 10^{-2}	7.5(± 3.1) × 10^{-2}
k_{a2}	6.7(± 1.8)	4.1(± 1.2)	10(± 5.9)
k_{d2}	1.5(± 0.58) × 10^{-3}	8.7(± 1.1) × 10^{-4}	9.3(± 1.1) × 10^{-4}
K_{D1} (= k_{d1}/k_{a1})	2.3(± 0.85) × 10^{-6}	7.9(± 7.1) × 10^{-6}	3.2(± 1.7) × 10^{-6}
K_{D2} (= k_{d2}/k_{a2})	2.4(± 0.71) × 10^{-4}	2.3(± 0.86) × 10^{-4}	1.1(± 0.67) × 10^{-4}
Species A (%[b])	27(± 3)	21(± 2)	26(± 1)
Species B (%[b])	46(± 2)	53(± 1)	36(± 1)
G5-MTX$_5$	High density	Intermediate density	[a] Low density
k_{a1}	9.9(± 1.1) × 10^3	1.1(± 0.1) × 10^4	7 × 10^3
k_{d1}	6.8(± 0.76) × 10^{-2}	1.9(± 0.5) × 10^{-1}	2 × 10^{-2}
k_{a2}	11(± 4)	17(± 8.1)	-
k_{d2}	3 × 10^{-3}	9.3(± 1.2) × 10^{-3}	-
K_{D1} (= k_{d1}/k_{a1})	6.9(± 1.5) × 10^{-6}	1.7(± 0.3) × 10^{-5}	9 × 10^{-6}
K_{D2} (= k_{d2}/k_{a2})	3.1(± 1.1) × 10^{-4}	6.2(± 2.6) × 10^{-4}	-
Species A (%[b])	20(± 5)	14(± 8)	≥95 (± 5)
Species B (%[b])	21(± 3)	8(± 1)	5

[a] Binding parameters derived from a single Langmuir fitting;

[b] Refers to the number of receptor sites occupied by dendrimer NPs relative to total number of the sites, and each of these values is an average from different injection concentrations